Energy fluxes in turbulent separated flows

Journal of Physics: Conference Series **759** (2016) 012003 doi:10.1088/1742-6596/759/1/012003

Energy fluxes in turbulent separated flows

J.-P. Mollicone, F. Battista, P. Gualtieri and C.M. Casciola

Department of Mechanical and Aerospace Engineering, Sapienza University of Rome

E-mail: carlomassimo.casciola@uniroma1.it

Abstract. Turbulent separation in channel flow containing a curved wall is studied using a generalised form of Kolmogorov equation. The equation successfully accounts for inhomogeneous effects in both the physical and separation spaces. We investigate the scale-by-scale energy dynamics in turbulent separated flow induced by a curved wall. The scale and spatial fluxes are highly dependent on the shear layer dynamics and the recirculation bubble forming behind the lower curved wall. The intense energy produced in the shear layer is transferred to the recirculation region, sustaining the turbulent velocity fluctuations. The energy dynamics radically changes depending on the physical position inside the domain, resembling planar turbulent channel dynamics downstream.

1. Introduction

Most of the statistical theory of turbulence concerns the mechanisms that sustain turbulent fluctuations against dissipation, namely production and fluxes of turbulent kinetic energy in the physical space [1] and across the different scales of motion [2]. In the classical picture, the energy flux and production are single point statistical observables unable to distinguish between the different scales of motion. On the other hand, the spectrum of turbulent kinetic energy and the spectral balance allow to address each scale of motion separately [3]. As a main drawback, the spectral description does not permit to localise the energy transfer process in space, due to projection on non-local Fourier modes. Physical and spectral views were already reconciled in the early stages of turbulent research, when Kolmogorov devised his description of turbulence in terms of structure functions. The implications of his extremely elegant and beautiful theory for inhomogeneous and complex flows was not recognised until recently through generalisations to shear dominated anisotropic flows.

The scale-by-scale approach, originally introduced by Kolmogorov to develop his theory in homogeneous and isotropic turbulence [5], has been progressively extended to anisotropic and inhomogeneous conditions, for example, from shear dominated flows, see [6, 7], to channel flow, see [8], [9] and [10]. Casciola et al. (2003) address the link between the intermittency and anisotropy in homogeneous shear flows [6]. The generalised Kolmogorov equation is then employed to distinguish the shear-dominated scales by the small isotropic scales dominated by dissipation. Numerical data shows that the dissipation scales are independent on the mean shear, so the intermittency correction is universal. Danaila et al. (2001) provide a generalised form of the Kolmogorov equation adding additional terms to account for the "large-scale turbulent diffusion acting from the walls through to the centreline of the channel" [8]. The aim is to apply the Kolmogorov theory to inhomogeneous turbulent flows with moderate Reynolds number. Hot-wire measurements allow the prediction of large scale effects on the dissipation rate at the

channel centre. The scale-by-scale budget in a planar turbulent channel flow is numerically studied by means the generalised form of Kolmogorov equation, see [9] and [10]. The DNS data sets are analysed to investigate how the inhomogeneity produced by the wall affects transfer of energy in physical and scale space at different distances from the wall. Such understanding is fundamental to tune innovative techniques to control boundary layer transition to turbulence or to design innovative turbulence models, see the discussion in [11], since it is able to capture the correct dynamics of the fluctuations for inhomogeneous flows.

The present work investigates, through Direct Numerical Simulation (DNS), the scale-by-scale energy production, transport and dissipation in a channel with a lower curved wall which is a relatively more complex geometry with respect to previous studies in homogeneous or shear flows. The results section shows how the generalised Kolmogorov equation is a viable tool to characterize the turbulence dynamics in anisotropic and strongly inhomogeneous flows. The energy can be transferred in the physical space from production regions (mainly the shear layer behind the bump) to regions where it is dissipated or alternatively, the energy produced in some specific region of the flow domain gives rise to an energy cascade in the separation spaces, depending on the distance from the wall.

2. Computational Approach

Direct numerical simulations are used to solve the incompressible Navier-Stokes equations,

$$\frac{\partial u_i}{\partial t} + u_j \frac{\partial u_i}{\partial x_j} = -\frac{\partial p}{\partial x_i} + \frac{1}{Re}\frac{\partial^2 u_i}{\partial x_j^2} + f_i \qquad \frac{\partial u_i}{\partial x_i} = 0, \tag{1}$$

where u_i is the i^{th} velocity component, p is the hydrodynamic pressure and f_i is the body force sustaining the flow inside the channel. $Re = h_0 U_b/\nu$ is the bulk Reynolds number, where h_0 is half the nominal channel height, U_b is the bulk velocity and ν is the kinematic viscosity. All length scales are made dimensionless with the nominal channel half-height, time with h_0/U_b and pressures with ρU_b^2. When needed, the adoption of wall units will be explicitly highlighted by the customary superscript $+$, and the index $i = 1, 2, 3$ will be replaced with the corresponding label, x, y or z. Angular brackets denote the temporal and z-direction averaging. The setup was simulated for enough time to reach steady state conditions before time-uncorrelated data sets were extracted for statistical analysis. The mesh contains approximately 120 million grid points. Large computational power was required for the simulation and therefore the simulation was run on the FERMI BlueGene/Q supercomputer located in Bologna, Italy. The computational fluid dynamics solver used is Nek5000 [12], which is based on the spectral element method (SEM), see [13].

Figure 1 shows a sketch of the simulated geometry. The curved wall inside the channel on the lower wall is commonly referred to as a "bump". The domain dimensions are $(L_x \times L_y \times L_z) = (26 \times 2 \times 2\pi) \times h_0$ where x, y, and z directions are the stream-wise, wall-normal and span-wise

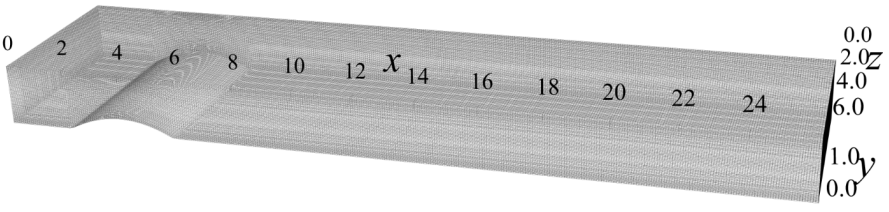

Figure 1. Sketch of the geometry of the channel with the curved lower wall.

directions respectively. Flow is from left to right in the x direction with periodic boundary conditions in both the streamwise, x, and spanwise, z, directions. No slip boundary conditions are enforced at the top and bottom walls. The simulation has a bulk Reynolds number equal to $Re = 2500$ and the maximum friction Reynolds number equal to $Re_\tau = u_\tau h_0/\nu = 300$.

3. The Generalised Kolmogorov Equation

The Kolmogorov equation follows directly from the equations of motion and describes all the dynamical effects occurring at each scale of the turbulent flow, see [14] and [15]. The generalised form of the Kolmogorov equation, in order to account for inhomogeneous conditions, is derived by [4], see also [16] and [17] for a different approach, and reads

$$\begin{aligned}
&\frac{\partial\langle\delta u^2\delta u_j\rangle}{\partial r_j}+\frac{\partial\langle\delta u^2\delta U_j\rangle}{\partial r_j}+\frac{\partial\langle\delta u^2 u_j^*\rangle}{\partial X_{cj}}+\frac{\partial\langle\delta u^2 U_j^*\rangle}{\partial X_{cj}}+\\
&2\langle\delta u_i\delta u_j\rangle\frac{\partial\delta U_i}{\partial r_j}+2\langle u_j^*\delta u_i\rangle\frac{\partial\delta U_i}{\partial X_{cj}}=\\
&-4\,\varepsilon^*+2\nu\frac{\partial^2\langle\delta u^2\rangle}{\partial r_j\partial r_j}+\frac{\nu}{2}\frac{\partial^2\langle\delta u^2\rangle}{\partial {X_{cj}}^2}+\frac{2}{\rho}\frac{\partial\langle\delta p\delta u_i\rangle}{\partial X_{ci}}\,.
\end{aligned}\tag{2}$$

Hereafter, any quantity denoted by an apostrophe indicates that is taken at x_i' which is a position separated by the vector $r_i = x_i' - x_i$ with respect to x_i. The coordinate of the mid-point between points x_i' and x_i is defined by $X_{c_i} = (x_i + x_i')/2$. Lower-case letters refer to fluctuations whilst upper-case letters refer to averaged quantities. The asterisk denotes the mid-point average, e.g. $u_i^* = (u_i' + u_i)/2$, whilst the δ denotes an increment, e.g. $\delta U_i = U_i' - U_i$.

Since the present domain has only one homogeneous direction, the span-wise one, the generalised Kolmogorov equation is defined in a five dimensions space where the independent coordinates are the two physical X_c and Y_c and the three separation r_x, r_y and r_z coordinates. In the simplified case of homogeneous turbulent flow, equation (2) reduces to the von Kármán equation, defined in the three dimensional separation space,

$$\frac{\partial\langle\delta u^2\delta u_i\rangle}{\partial r_i}=-4\,\varepsilon^*+2\nu\frac{\partial\langle\delta u^2\rangle}{\partial r_i\partial r_i}\,.\tag{3}$$

In order to highlight the physical description of each single term of equation (2), the generalised Kolmogorov equation can be recast as follow,

$$\left(\frac{\partial\Phi_{r,j}}{\partial r_j}+\frac{\partial\Phi_{c,j}}{\partial X_{cj}}\right)=-4\,\varepsilon^*-(\Pi_r+\Pi_c)\,,\tag{4}$$

where ε is the turbulent kinetic energy dissipation, Π_r and Π_c are the energy production in the separation and physical spaces respectively,

$$\Pi_r=2\langle\delta u_i\delta u_j\rangle\frac{\partial\delta U_i}{\partial r_j}\tag{5}$$

$$\Pi_c=2\langle u_j^*\delta u_i\rangle\frac{\partial\delta U_i}{\partial X_{cj}}\,,\tag{6}$$

and $\Phi_{r,j}$ and $\Phi_{c,j}$ are the energy flux in the separation and physical spaces respectively,

$$\Phi_{r,j}=\langle\delta u^2\delta u_j\rangle+\langle\delta u^2\delta U_j\rangle+2\nu\frac{\partial\langle\delta u^2\rangle}{\partial r_j}\tag{7}$$

$$\Phi_{c,j}=\langle\delta u^2 u_j^*\rangle+\langle\delta u^2 U_j^*\rangle+\frac{\nu}{2}\frac{\partial\langle\delta u^2\rangle}{\partial X_{cj}}+\frac{2}{\rho}\frac{\partial\langle\delta p\delta u_j\rangle}{\partial X_{cj}}\,.\tag{8}$$

Equation (4) provides a way to distinguish between the transfer of energy from production to dissipation in both physical and separation spaces as opposed to only observing one-point statistics, as, for example, in the mean flow kinetic energy and the turbulent kinetic energy equations, which provide information concerning the transport, production and dissipation only in physical space.

4. Results

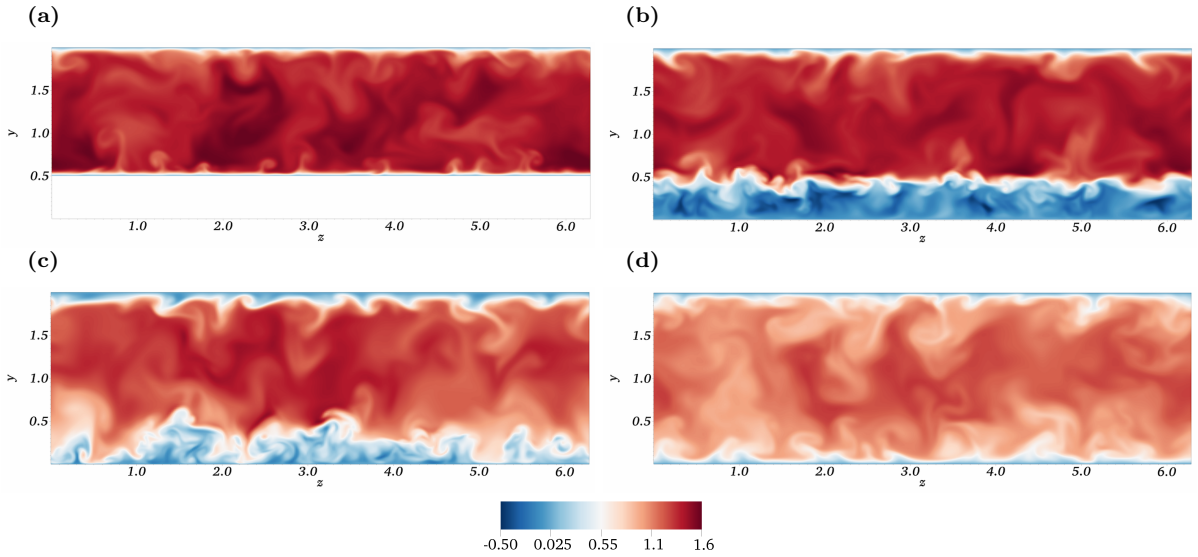

Figure 2. Instantaneous streamwise velocity contour plots in y-z planes at the tip of the bump in panel (a), end of the bump in panel (b), towards the end of the separation bubble in panel (c) and at $x = 24$ in panel (d).

Figure 2 shows instantaneous streamwise velocity contour plots in y-z planes at various x locations inside the domain. Panel (a) shows the flow at the tip of the bump, where the boundary layer becomes thinner towards the lower wall due to the intense flow acceleration induced by the decrease in channel section. At the end of the bump, panel (b), the separation induced by the abrupt change in channel section increase is evident and an intense shear layer detaches from the bump separating the recirculation bubble from the bulk flow. The shear layer is corrugated by large scale structures. Effects on the top wall are seen by the thickening of the boundary layer which is more evident further downstream towards the end of the separation bubble, panel (c), where the flow reattaches to the bottom wall. The flow stabilises downstream at $x = 24$, panel (d), where it resembles a classical planar turbulent channel flow.

Figure 3 shows a vorticity iso-surface which highlights the turbulent structures just behind the bump. Small three-dimensional structures that fill the recirculation region in the bottom half of the channel are generated by the shear layer. These structures tend to disappear downstream and elongated structures, similar to the planar channel streaky structures, appear close to the walls. Figure 4 shows the contour plots of mean streamwise velocity. The separation bubble behind the bump is evident and a smaller stagnation region in front of the bump is also present. Due to the diminished channel section at the bump, the flow accelerates. The contour plot confirms the existence of a strong shear layer between the bulk flow and the separation bubble. As anticipated, the bump also affects the flow close to the top wall where boundary layer thickening occurs.

Figure 3. Instantaneous vorticity surfaces at constant magnitude.

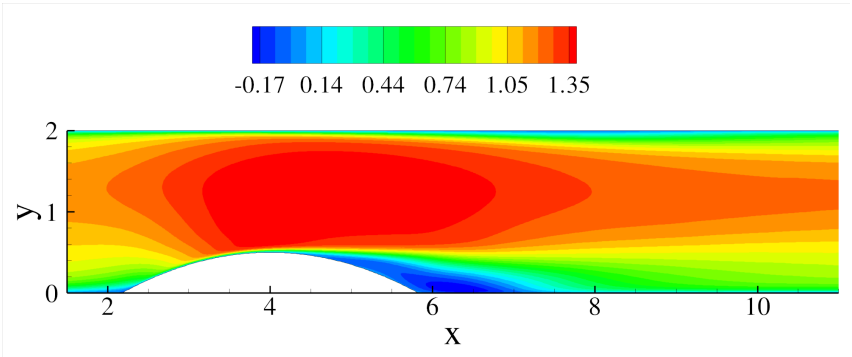

Figure 4. Contour plot of the streamwise mean velocity. Only a small portion of the flow domain near the bump is shown.

Energy fluxes, production and dissipation are now discussed following the background provided in section 3. We recall that the proper phase space involves five dimensions, namely three separations and two center point positions. The results discussed in the following concern the two-dimensional sub-spaces (Y_c, r_z) at fixed streamwise stations X_c with $r_x = r_y = 0$, see figure 5. Figure 6 reports the energy fluxes, Φ_r and Φ_c, as vectors and the right-hand side of equation (4) as background contour plots. All the terms in equation (2) are normalised with the dissipation $-4\varepsilon^*$ and, for better visualisation, the vectors are shown in arbitrary units. Proceeding downstream from panel (a) to panel (f) in figure 6, the energy dynamics shows a substantial dependence on the streamwise position X_c. Three main regions can be distinguished: the zone before the bump in panel (a), the zone after the bump where the flow is separated in panels (b)-(d) and the well reattached flow region downstream in panel (f).

In panel (a), the intense localised production at small scales, $r_z^+ \approx 50$, and close to the wall, $y^+ \approx 25$, is associated with the small recirculation just ahead of the bump. In this plane, the wall-normal component of the spatial flux, $\Phi_{c,y} = \langle \delta u^2 u_y^* \rangle + \langle \delta u^2 U_y^* \rangle + \frac{\nu}{2} \partial \langle \delta u^2 \rangle / \partial X_{cy} + \frac{2}{\rho} \partial \langle \delta p \delta u_y \rangle / \partial X_{cy}$, is dominated by the contribution arising from the mean flow and overwhelms the r_z-component of the flux, $\Phi_{r,r_z} = \langle \delta u^2 \delta u_z \rangle + 2\nu \partial \langle \delta u^2 \rangle / \partial r_z$. The physical interpretation is that energy generated near the wall is moved towards the center of the channel. We observe that the fluxes apparently do not absorb all the energy produced by the localised source, suggesting

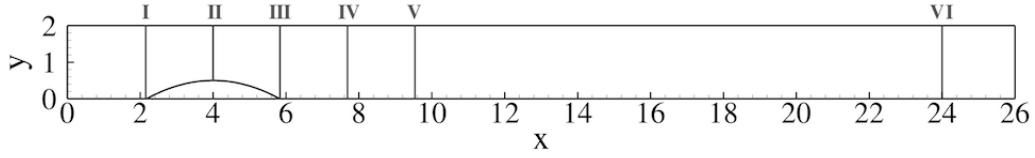

Figure 5. Sketch of the stream-wise stations selected for the statistical analysis.

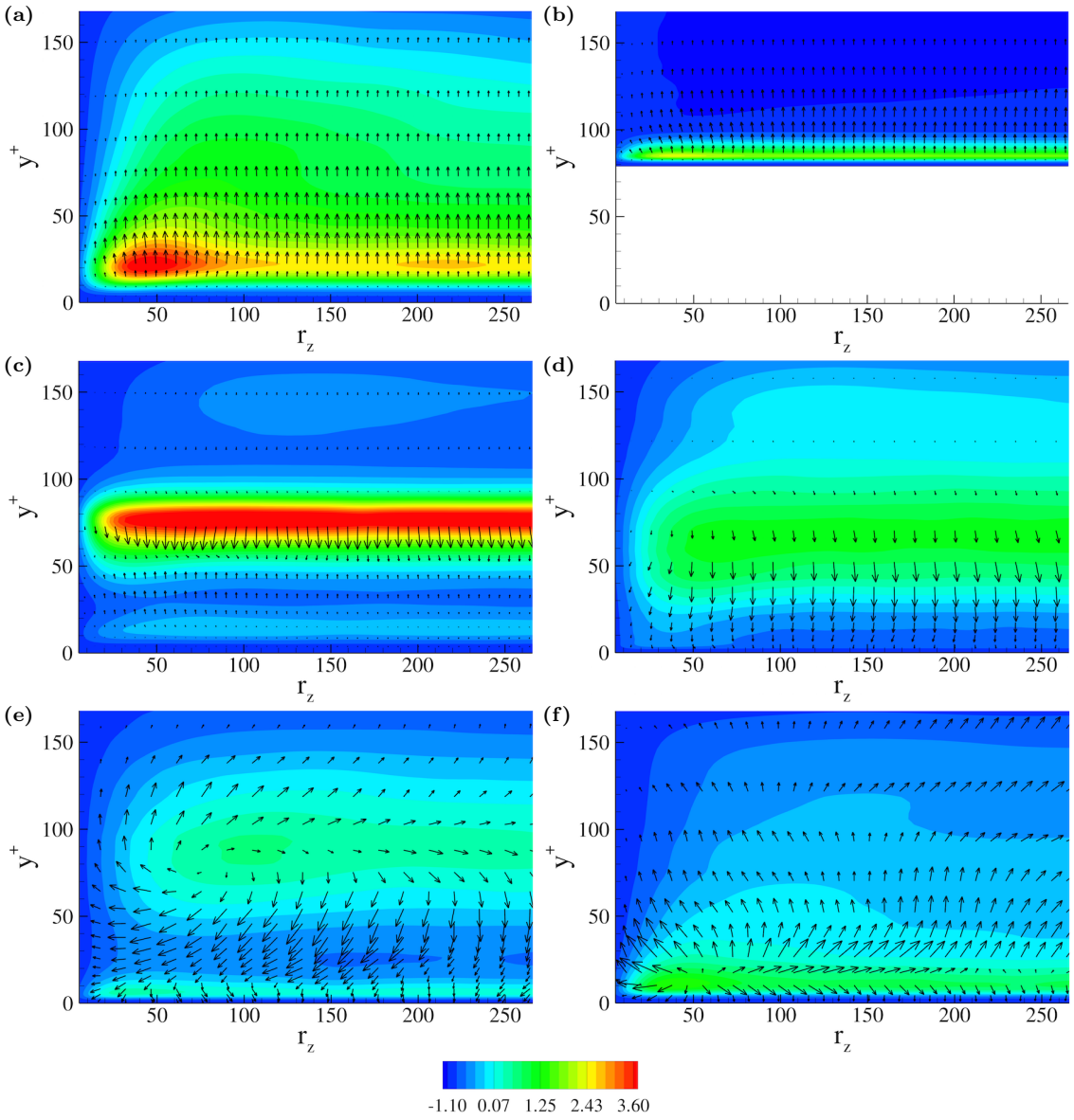

Figure 6. Contour plots of $(\Pi - 4\epsilon^*)/(4\epsilon^*)$ with vectors representing Φ in the reduced space (Y_c, r_z), i.e. in the plane $r_x = r_y = 0$, $X_c = const.$ Panels (a) to (f) represent stations I to VI respectively, see Figure 5. Only the lower half of the channel, where the bump is present, is shown.

that the excess energy is captured by the other components of the flux acting in directions orthogonal to the plane.

At the tip of the bump, panel (b), production occurs across all the scales, the qualitative behaviour of the fluxes is basically unchanged, and again, the energy produced at a given spanwise separation is moved by the spatial flux towards the center of the channel.

The most interesting behaviour occurs downstream, after the bump, where the interaction of the main bulk flow and the recirculation bubble produces an intense shear layer. Energy production is intense over a large range of scale separations, for $r_z^+ > 20$, and is spatially located at $y^+ \simeq 75$ which corresponds to the position of the shear layer away from the wall. Apart from the intense energy production due to the shear layer, a second, small intensity local peak (light

blue) of $\Pi - 4\epsilon^*$ can be observed close to the bottom wall deep inside the recirculating region. These two regions of production (the shear layer and the second minor peak) feed energy to the recirculating region. The absence of a significant r_z-component of the flux suggests that the fluid structures do not change their spanwise size.

Downstream, the most intense energy production peak gradually decreases while the second peak close to the bottom wall becomes more prominent and stabilises to turbulent channel-like behaviour in panel (f). The energy behaviour in panel (f) is in accordance with what already observed in the literature [10]. The downstream evolution from panels (d) to panels (e) shows the change between fluxes directed towards the wall inside the recirculation bubble below the shear layer and fluxes directed towards the channel center downstream of the bubble. In particular, in panel (e), the fluxes take a clockwise orientation as the r_z-component rises in intensity, indicating a transfer of energy to smaller spanwise scales below the nominal position of the shear layer and to larger scales above.

5. Conclusions

Turbulent separation was addressed by a Direct Numerical Simulation of turbulent channel flow with a lower curved wall. The presence of the bump produces a stable, fully turbulent recirculation bubble which is separated from the core flow by a strong shear layer.

This configuration is sufficiently general to reproduce the general features of separated flows, yet it is simple enough to allow to explore the potential of novel advanced statistical tools for turbulence dynamics. In particular, new partial results were discussed concerning the generalised Kolmogorov equation which, up to now, was only used to deal with simpler configurations where no separation occurs. The Kolmogorov equation allows to study the energy dynamics not only in the physical space but also in the separation space, i.e. it extends the scale-by-scale budget originally used by Kolmogorov to characterise the homogeneous and isotropic turbulence.

The channel section variation induced by the lower curved wall greatly affects the energy transfer across different scales and positions. The most intense peak of energy production is found in the shear layer where strong velocity fluctuations and intense mean velocity gradients occur. Production and dissipation of energy are not uniform throughout both physical and separation spaces. The scale-by-scale analysis is found able to account for the inhomogeneous effects coming from the recirculation region. It highlights how the turbulent fluctuations behind the bump are sustained by spatial energy fluxes arising from the shear layer to feed the recirculation bubble. Although the presented results provide a partial view, the analysis can be extended to cover all the five components of scale and spatial fluxes and their relationships with production and dissipation in turbulent flow separation.

Acknowledgments

The research leading to these results has received funding from the European Research Council under the ERC Grant Agreement no. 339446. PRACE, under grant no. 2014112647, has awarded access to resource FERMI based in Bologna, Italy.

References

[1] Townsend A 1976 *Cambridge UP, Cambridge*
[2] Frisch U 1995 *Turbulence: the legacy of AN Kolmogorov* (Cambridge university press)
[3] Monin A and Yaglom A 1971 *Vol. I and II MIT Press, Cambridge*
[4] Hill R J 2002 *Journal of Fluid Mechanics* **468** 317–326
[5] Kolmogorov A N 1941 *Dokl. Akad. Nauk SSSR* vol 30 pp 299–303
[6] Casciola C M, Gualtieri P, Benzi R and Piva R 2003 *Journal of Fluid Mechanics* **476**
[7] Casciola C, Gualtieri P, Jacob B and Piva R 2005 *Physical review letters* **95** 024503
[8] Danaila L, Anselmet F, Zhou T and Antonia R 2001 *Journal of Fluid Mechanics* **430** 87–109
[9] Marati N, Casciola C M and Piva R 2004 *Journal of Fluid Mechanics*

[10] Cimarelli A, Angelis E D and Casciola C M 2013 *Journal of Fluid Mechanics* **715**
[11] Thiesset F, Antonia R A, Danaila L and Djenidi L 2013 *Physical Review E* **88** 011003
[12] Fischer P, Lottes J W and Kerkemeier S G Nek5000 - Open source spectral element CFD solver. Argonne National Laboratory, Mathematics and Computer Science Division, Argonne, IL, see http://nek5000.mcs.anl.gov (2008).
[13] Patera A T 1984 *Journal of Computational Physics* **54** 468–488
[14] Thiesset F, Danaila L and Antonia R A 2014 *Fluid-Structure-Sound Interactions and Control*
[15] Cambon C and Gracia B J 2013 *Journal of Turbulence*
[16] Yakhot V 2001 *Physical Review E* **63** 026307
[17] Kurien S and Sreenivasan K R 2001 *Physical Review E* **64** 056302